Nuclear astrophysics studies with the Trojan Horse Method

Aurora Tumino[1,2]

[1]Dipartimento di Ingegneria e Architettura, Università degli Studi di Enna “Kore", Enna, Italy
[2]INFN-Laboratori Nazionali del Sud, Catania, Italy

Abstract. Our understanding of how stars evolve relies on two critical factors: energy production and chemical evolution. These factors are influenced by thermonuclear reactions. However, directly measuring these reactions in a laboratory setting can be challenging due to small reaction cross sections or the need for radioactive targets that are impractical to handle.
To overcome these challenges, scientists have developed indirect techniques. One such method is the Trojan Horse Method (THM), which utilizes transfer reactions to determine cross sections of reactions relevant to stellar burning processes. In this paper, we will delve into the features of the Trojan Horse Method, its application in nuclear astrophysics, and provide examples of THM measurements.

1 Introduction

Studying the fusion of elements within stars presents a significant challenge due to the Coulomb repulsion between atomic nuclei. This repulsion causes the reaction cross section, $\sigma(E)$, to dramatically decrease at the low energies typically found inside stars. When direct measurement is not feasible, scientists often extrapolate the behavior of $\sigma(E)$ at low energy from higher energies (usually E>100 keV) using the astrophysical S(E)-factor

$$S(E) = E\sigma(E)\exp(2\pi\eta), \tag{1}$$

here η the Coulomb parameter of the colliding nuclei, and $\exp(2\pi\eta)$ accounts for the Gamow factor that mitigates the Coulomb suppression of $\sigma(E)$ due to barrier tunneling. Uncertainties arise when attempting to determine the fusion rate at stellar energies, such as unexpected resonances or the influence of electron screening. In laboratory settings, both target and projectile nuclei are typically surrounded by electrons from atoms or molecules. These electron clouds act as a shield, reducing the Coulomb repulsion between the nuclei—a phenomenon known as "electron screening." As a result, the fusion reaction cross section for screened nuclei, $\sigma_s(E)$, is larger compared to that of bare nuclei, $\sigma_b(E)$, [1, 2]. To account for this screening effect and determine the bare nucleus cross section, scientists introduce the screening factor:

$$f_{\rm lab}(E) = \sigma_s(E)/\sigma_b(E) \approx \exp(\pi\eta U_e/E)\,, \tag{2}$$

where U_e, the so-called "electron screening potential" [2, 3], has to be taken into account to determine the bare nucleus cross section.
In stellar plasmas, a similar enhancement factor relates the cross section σ_{pl}(E) to the bare nucleus cross section:

$$f_{pl}(E) = \sigma_{pl}(E)/\sigma_b(E) \approx \exp(\pi\eta U_{pl}/E) \tag{3}$$

that can be calculated by knowing the plasma screening potential U_{pl}, that in turn depends on important properties of the plasma such as the Debye-Hückel radius.

Understanding electron screening in laboratory experiments contributes to a better comprehension of U_{pl}. Interestingly, experiments on low-energy fusion reactions have confirmed the expected exponential increase in reaction rates predicted by Equation (2) [2]. However, a surprising result has emerged. The calculated U_e values from these experiments are consistently higher than what traditional atomic models predict (adiabatic limit). These models estimate U_e based on the difference in electron binding energies between the separate atoms in the entrance channel and that of the composite atom [2, 3]. This discrepancy between theory and experiment, observed in lab measurements, remains unexplained. A week point in the laboratory approach - and thus in the deduced U_e value - is the necessity to make an assumption for the energy dependence of σ_b(E) at ultra-low energies. To overcome these limitations, indirect techniques have been developed, as described in ([4, 5] and references therein). One such powerful method is the Trojan Horse Method (THM) ([6, 7] and references therein).

The THM offers a reliable alternative path to directly measure σ_b(E) for reactions involving charged particles. In this paper, the core concepts of the THM will be presented, showcasing some recent successful applications of this method.

2 Basics of the Trojan Horse Method

The THM ([7] and references therein) is a technique used to measure the astrophysical two-body reaction, denoted as $A + x \rightarrow c + C$, by exploiting a suitable two-to-three body process, $A + a \rightarrow c + C + s$. The THM takes advantage of the

relationship between these two reactions based on nuclear reaction theories.

In the three-body reaction, the target a (or projectile) exhibits a wave function that has a significant amplitude for a $x - s$ cluster configuration. Here, x represents the target (or projectile) involved in the two-body reaction. The experiment explores the three-body phase space where quasi-free kinematics applies, with the other cluster s acting as a spectator. The reaction $A + x \rightarrow c + C$ can be viewed as a half-off-energy-shell (HOES) two-body reaction, commonly referred to as the quasi-free reaction. As this three-body process occurs above the Coulomb barrier, both the Coulomb barrier and screening effects are suppressed in the HOES two-body cross section. However, even at very low sub-Coulomb energies, the quasi-free $A + x$ process can occur due to compensation between the relative motion of $A + a$ and the binding energy of the $x - s$ system. To determine the accessible astrophysical energy range, the intercluster motion plays a crucial role, leading to a momentum distribution cutoff of s at a few tens of MeV/c. In this context, the "quasi-free two-body energy" is defined as:

$$E_{QF} = \frac{m_x}{m_x + m_A} E_A - B_{x-s}. \tag{4}$$

Here, E_A represents the beam energy, m_x and m_A are the masses of x and A particles, respectively, and B_{x-s} is the binding energy of the $x - s$ system. In the Impulse Approximation, which neglects the interaction of the spectator with particles C and c, the three-body cross section can be factorized as:

$$\frac{d^3\sigma}{dE_c d\Omega_c d\Omega_C} \propto [KF\ |\varphi_a(\mathbf{p}_{sx})|^2] \left(\frac{d\sigma}{d\Omega_{c.m.}}\right)^{\mathrm{HOES}} \tag{5}$$

where KF is a kinematical factor containing the final state phase-space factor. It is a function of the masses, momenta and angles of the outgoing particles; $\varphi_a(\mathbf{p}_{sx})$ is proportional to the Fourier transform of the radial wave function $\chi(\mathbf{r})$ for the $x - s$ inter-cluster relative motion; $(d\sigma/d\Omega_{c.m.})^{\mathrm{HOES}}$ is the half-off-energy-shell (HOES) differential cross section for the binary reaction at the center of mass energy $\mathrm{E}_{c.m.}$ given in post-collision prescription by

$$E_{c.m.} = E_{cC} - Q_{2b}\ . \tag{6}$$

Here, Q_{2b} is the Q-value of the binary reaction and E_{cC} is the relative energy of the outgoing particles c and C, which spans the accessible astrophysical region defined above.

In the factorization of Eq.5, $\varphi_a(\mathbf{p}_{sx})$ is taken from the experiment, allowing for possible deviations from the pure Plane Wave Impulse Approximation. This factorization affects only the absolute magnitude of the cross section but not its energy dependence.

3 Experimental approach

Experimental procedures in Trojan Horse Method (THM) typically involve a straightforward reconstruction of particle kinematics. The exit channel, consisting of two of the three particles (commonly denoted as c and C) resulting from the virtual two-body reaction of interest, is detected and identified using telescopes placed in a phase space region dominated by quasi-free kinematics. The detection setup usually includes silicon detectors or ionization chambers as ΔE detectors and position-sensitive detectors (PSD) as E detectors. Once the reaction channel is selected, a crucial step is to separate the quasi-free mechanism from other reaction mechanisms that produce the same particles in the final state, such as sequential decay and direct break-up. One observable that provides insight into the reaction mechanism is the shape of the experimental momentum distribution of the spectator particle, denoted as $\varphi_a(\mathbf{p}_{sx})$. To reconstruct the experimental $\varphi_a(\mathbf{p}_{sx})$ distribution for each pair of coincidence QF angles, the quasi-free coincidence yield is divided by the kinematic factor. This yields a quantity proportional to the product of the momentum distribution for the spectator particle and the differential two-body cross section. The range for this division (or window) is chosen such that the differential two-body cross section within that range can be considered approximately constant. Therefore, the resulting quantity represents the momentum distribution for the spectator particle, which in the Plane Wave Impulse Approximation (PWIA) can be compared with the Fourier transform of the radial $x - s$ bound state wave function.
Data analysis is typically limited to the region where the agreement between the two distributions exists. Usually a window of few tens of MeV/c is chosen not to move too far from E_{QF}, according to the prescriptions reported in [13].
Therefore, $((d\sigma/d\Omega_{cm})^{\mathrm{HOES}}$ can be extracted from the three-body coincidence yield by simply inverting Eq.5. The Coulomb barrier in $((d\sigma/d\Omega_{cm})^{\mathrm{HOES}}$ is suppressed [8] which is attributed to the virtuality of particle x. This suppression has also been observed in scattering processes. For example, the $p + p$ elastic scattering through the $^2\mathrm{H}(p, pp)n$ reaction has been studied [10, 11]. The $p + p$ system is the simplest system where Coulomb and nuclear forces co-exist and are coherent. Coherence means interference, which is destructive due to the opposite sign of the two forces. Interference is responsible for the deep minimum in the free $p + p$ cross section shown in Fig.1 as solid line as a function of the $p - p$ relative energy E_{pp}. The extracted $p - p$ HOES cross section is shown as black and colored symbols. The dashed-dotted line represents the calculated HOES $p-p$ cross section as reported in [10, 11] where the Coulomb amplitude is strongly suppressed compared to the nuclear one. We observe a striking disagreement between the THM (HOES) and the OES $p - p$ cross sections throughout the region of the interference minimum, which is missing in the THM data. Instead, the calculated HOES $p-p$ nicely fits the THM data. A full account of the work is reported in [10, 11]. The good agreement provides conclusive evidence of the suppression of Coulomb effects in the THM method.
To relate the HOES excitation function to the relevant OES one, Coulomb corrections must be taken into account. For angular distributions, no correction is necessary as it would introduce a simple scaling factor when the energy is

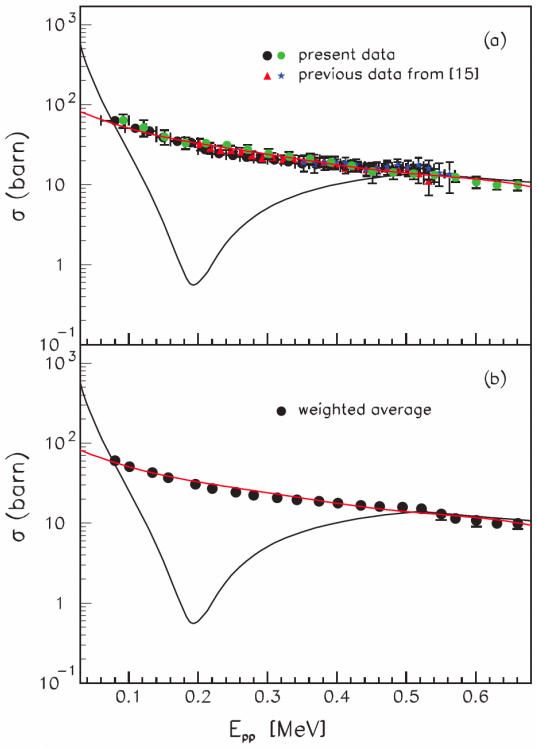

Figure 1. (a) THM two-body cross section (black and colored symbols) vs.pp relative energy (E$_p p$) [10, 11]. Solid line represents the theoretical on-energy-shell (OES) p-p cross section [12]. The dashed-dotted line is the calculated HOES cross section [10, 11]. (b) Weighted average of all the experimental data shown in (a) vs. E$_p p$ with the same meaning for the solid lines as above.

fixed. Thus, the OES data can be directly compared with the HOES data projected onto the emission angle of C (or c) in the $C-c$ center-of-mass system, denoted as $\theta_{c.m.}$, using the formula provided in [14]:

$$\theta_{c.m.} = \arccos \frac{(\mathbf{v}_A - \mathbf{v}_x) \cdot (\mathbf{v}_c - \mathbf{v}_C)}{|\mathbf{v}_A - \mathbf{v}_x||\mathbf{v}_c - \mathbf{v}_C|} \quad (7)$$

where the vectors $\mathbf{v}_A$, $\mathbf{v}_x$, $\mathbf{v}_c$, $\mathbf{v}_C$ are the velocities of projectile, transferred particle and outgoing nuclei respectively. These quantities are calculated from their corresponding momenta in the lab-system, where the momentum of the transferred particle is equal and opposite to that of s when the quasi-free break-up takes place in the target, otherwise a little different formula has to be used [14]. If HOES data are projected onto the E$_{Cc}$ axis, Coulomb suppression has to be introduced before comparison with OES data. In a simple approach this is done by means of the penetrability factor:

$$P_l(k_{Ax}R) = \frac{1}{G_l^2(k_{Ax}R) + F_l^2(k_{Ax}R)} \quad (8)$$

with F_l and G_l regular and irregular Coulomb wave functions and R the so called cutoff radius [18], which is usually chosen as the sum of the radii of nuclei A and x. This procedure prevents us to extract the absolute value of the two-body cross section. However, this is not a real problem since the absolute magnitude can be derived from a scaling to the direct data available at higher energies. data available at higher energies.

For resonant two-body reactions, the $(d\sigma/d\Omega_{c.m.})^{\mathrm{HOES}}$ cross section needs to be determined to obtain the corresponding OES S(E) factor. Recently, a rigorous theoretical formalism called modified R-matrix approach has been developed [19] to account for HOES effects resulting from the virtual nature of particle x. By fitting the experimental THM cross section, the reduced width amplitude γ for entrance and exit channels, energy levels and energy shifts can be deduced and used to determine the astrophysical S(E) factor, since these parameters are the same in both direct and THM data. In this way, an exact parameterization of the astrophysical S(E) factor can be obtained overcoming the extrapolation. If the resonance parameters of a single level in the relevant energy region are known, they can be fixed in the fitting procedure to obtain directly the astrophysical S(E) factor in absolute units.

Several test studies have been performed in the past years to validate the THM, such as the invariance of the two-body reaction amplitude with changing the Trojan Horse nucleus hiding the participant cluster x [20–22], or the use of momentum distributions from Distorted Wave Born Approximation instead of the simple PWIA shape, providing same results within experimental errors [25, 50, 52]. The THM has been applied to many reactions of astrophysical interest connected to fundamental problems in different scenarios, from BBN nucleosynthesis [18, 26–28, 31–46, 48] to AGB and more explosive sites [49–62]. Recently, reactions involving heavier systems, such as ^{12}C and ^{16}O have been investigated [63].

4 Applications: The ^{12}C+^{12}C fusion at astrophysical energies

The fusion of carbon isotopes, specifically ^{12}C+^{12}C, plays a crucial role in various scenarios involving carbon-rich environments. This process has significant implications in different nuclear fields and has been extensively studied. It has been found to be influential in star evolution and the nucleosynthesis of intermediate mass and massive stars ($\geq$8 M$_\odot$) [64]. Additionally, it determines the lower stellar mass limit for carbon ignition and provides constraints for models involving superbursts with neutron and strange stars, in particular if resonances are found to contribute in the Gamow peak [65]; The ^{12}C+^{12}C fusion also affects the weak component of the s process, which is responsible for the production of elements between Fe and Sr. Hydrostatic carbon burning occurs at temperatures ranging from 0.8 to 1.2 GK, corresponding to sub-Coulomb center-of-mass energies from 1 to 3 MeV. The cross section for this fusion process decreases rapidly below the nanobarn range, making measurements challenging, particularly below a center-of-mass energy (E$_{cm}$) of 2 MeV. The compound nucleus ^{24}Mg is formed at an excitation

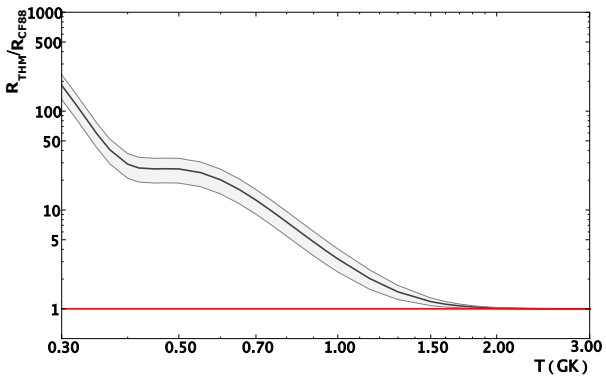

Figure 2. Ratio between the total THM ^{12}C+^{12}C reaction rate (black line) and the reference one (red line) from [68] referred to as CF88. The grey shading defines the region spanned owing to the $\pm 1\sigma$ uncertainties.

energy above the particle decay threshold. Alpha, proton and neutron are the dominant evaporation channels, leading respectively to ^{20}Ne, ^{23}Na and ^{23}Mg, which can also be produced in excited bound states. Below 2.5 MeV there is not enough energy to feed ^{23}Mg even in its ground state and α and p channel are the only relevant ones at low energies.

In order to determine the cross section at these energies, an indirect measurement approach was employed. The ^{12}C(^{12}C,α)^{20}Ne and ^{12}C(^{12}C,p)^{23}Na reactions were studied via the Trojan Horse Method (THM) applied to the ^{12}C(^{14}N,α^{20}Ne)^{2}H and ^{12}C(^{14}N,p^{23}Na)^{2}H three-body processes in the quasi-free kinematics regime, where ^{2}H from ^{14}N is spectator to the ^{12}C+^{12}C two-body processes [63]. This method allowed for the extraction of the astrophysically relevant two-body cross section for four channels: ^{20}Ne+α_0, ^{20}Ne+α_1, ^{23}Na+p_0, and ^{23}Na+p_1. The experimental setup involved utilizing telescopes equipped with detectors to detect the ejectile (either α or proton) in coincidence with the spectator deuteron particle.

The data analysis involved several steps, as described in the reference [63]. The resulting cross sections were used to determine the S(E) factors for the four reaction channels. The resonance structure observed in the excitation functions of these reactions is consistent with known resonance energies of ^{24}Mg reported in the literature. The modified R-matrix analysis took into account the relevant resonances and neglected contributions from channels other than those of interest. The resulting reaction rate, shown in Fig. 2, exhibits a variation with temperature, with an increase from a factor of 1.18 at 1.2 GK to more than 25 at 0.5 GK. This increase is mainly attributed to the resonant structure around $E_{c.m.}$=1.5 MeV and supports the theoretical conjecture that the superburst ignition depths in accreting neutron stars can be reduced by a factor of 2, based on the observed change in the fusion rate.

As for the hydrostatic carbon burning regime (0.6 to 1.2 GK), the present rate change will lower temperatures and densities at which ^{12}C ignites in massive post-main-sequence stars. Profiting of the stellar modeling reported in [68], for core C-burning of a star of 25$M_\odot$, the ignition temperature and density would undergo a decrease of down to 10% and 30% respectively.

The impact of the new carbon fusion cross section extends beyond stellar evolution. It has implications for Type Ia Supernovae and the progenitors of CO white dwarfs and normal type II supernovae [69]. The measurement of ^{12}C+^{12}C through the THM affects the ignition temperature of carbon burning, potentially leading to increased occurrences of accretion-induced collapse and the birthrate of Galactic neutron stars. Furthermore, it influences the upper bound for the mass of progenitors of CO white dwarfs and the lower bound for the mass of progenitors of normal type II supernovae [70]. Recent investigations also reveal significant modifications in the correlation between compactness and initial mass of stars during core collapse, which could impact the occurrence of a stellar explosion [71]. Specifically, we analyzed how this measurement impacts the binding energy of the inner mantle during the initiation of core collapse. The outcomes reveal a significant modification in the correlation between compactness and initial mass, contrasting with previous findings derived from the conventional reference cross section provided in Caughlan & Fowler [67] referred to as CF88. This occurrence holds potential implications regarding the occurrence of a stellar explosion.

5 Applications: The Coulomb free $p-p$ scattering cross-section and $^1S_0$ scattering length

Recently, we utilized the quasi-free scattering of protons below 1 MeV, as described in references [10, 11], to obtain the first experimental determination of the Coulomb-free scattering length and effective range for $p-p$ interactions in the $^1S_0$ channel [72]. Our approach relied on a crucial aspect of the reaction, namely the suppression of Coulomb effects in the extracted two-body cross section at energies below the Coulomb barrier, as well as the application of the concept of a universal window, which is applicable to the nucleon-nucleon (NN) system. By employing a Bayesian data-fitting technique using the expression of the s-wave NN scattering cross section, we obtained a scattering length of $a_{pp} = -18.17^{+0.52}_{-0.58}|_{stat} \pm 0.01_{syst}$ fm and effective range $r_0 = 2.80 \pm 0.05_{stat} \pm 0.001_{syst}$ fm. Results are reported in Fig. 3. The experimental quasi-free p-p scattering cross section after removal of the residual Coulomb interaction (black solid circles) has been obtained by the weighted average of the datasets reported in [12] and shown in Fig. 1(b).

To extract meaningful information about charge symmetry breaking in short-range interactions, we relied on the notion that the NN phase shift δ in traditional analyses of NN scattering data at low energies, captures all the effects of short-range interactions. Additionally, we developed a model based on universality concepts to aid in the interpretation of the results. As a result, we concluded that this technique provides us with parameters that enable the assessment of charge symmetry breaking in the entirety of

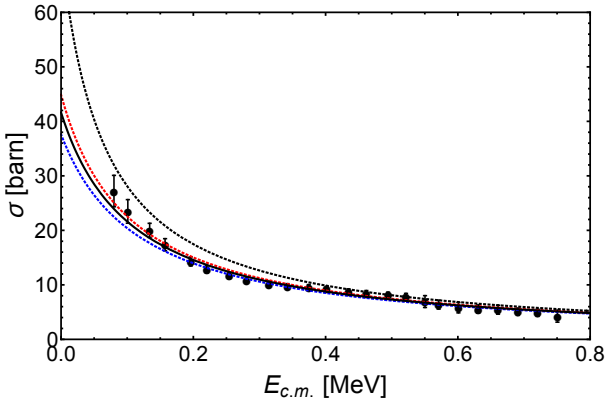

Figure 3. Experimental quasi-free p-p scattering cross section after removal of the residual Coulomb interaction (black solid circles). Error bars indicate $\pm 1\sigma$ uncertainties. The result of the fit using Eq. (3) of [72] is shown as solid black line, while the dotted red, blue and black lines refer to Eq. (3) for n-n, p-p and n-p scatterings, respectively, using current accepted values for nuclear a and r_0 parameters.

the short-range interaction. Our results indicate that the impact of the different up-down quark masses and residual electromagnetic properties has a limited effect on charge symmetry breaking. This finding leads us to propose a new paradigm for the study of charge symmetry breaking, aligning with the current understanding that, at a fundamental level, the charge dependence of nuclear forces arises from the difference in masses between up and down quarks and the electromagnetic interactions among them.

6 Conclusions

The THM has emerged as a valuable and versatile technique for investigating nuclear reactions that are not only relevant to astrophysical processes but also have broader applications. This method provides a means to study low-energy reactions that are typically challenging or hindered by other experimental approaches. It is important to note that the application of THM requires meticulous data analysis to ensure accurate results. One of the unique strengths of the THM lies in its ability to probe reaction channels involving nuclei in their ground states, obviously not accessible through γ-particle coincidence. Looking ahead, the THM is expected to find further applications in both experimental and theoretical contexts.

References

[1] H.J. Assenbaum *et al.*, Z. Phys. A **327**, 461 (1987)
[2] F. Strieder *et al.*, Naturwissenschaften **88**, 461 (2001)
[3] G. Fiorentini *et al.*, Z. Phys. A **350**, 289 (1995)
[4] A. Tumino *et al.*, Few Body Syst. **54**, Issue 7-10, 869 (2013)
[5] R. E. Tribble, *et al.*, Rep. Prog. Phys. **77**, 106901 (2014)
[6] R.G. Pizzone *et al.*, Eur. Phys. J. A **56**, 283 (2020)
[7] A. Tumino, *et al.*, Ann. Rev. Nucl. Part. Sci. **71**, 345 (2021)
[8] A.M. Mukhamedzhanov *et al.*, Eur. Phys. J.A **27**, 205 (2006)
[9] A. Tumino *et al.*, Eur. Phys. J. A **25**, 649 (2005)
[10] A. Tumino *et al.*, Phys. Rev. Lett. **98**, 252502 (2007)
[11] A. Tumino *et al.*, Phys. Rev.C **78**, 064001 (2008)
[12] J.D. Jackson and J.M. Blatt, Rev. Mod. Phys. **22**, 77 (1950)
[13] I.S. Shapiro *et al.*, Nucl. Phys. A, **61**, 353 (1965)
[14] M. Jain *et al.* , Nucl. Phys. A **153**, 49 (1970)
[15] C.J. Copi, D.N. Schramm, M.S. Turner, Science **627**, 192 (1995)
[16] M. Lattuada *et al.*, Astrophysical Journal **562**, 1076 (2001)
[17] A. Tumino *et al.*, Eur. Phys. J. A direct (2006), 1 DOI: 10.1140/epja/i2006-08-038-1
[18] A. Tumino *et al.*, Phys. Rev.C **67**, 065803 (2003)
[19] A.M. Mukhamedzhanov, Phys. Rev.C **84**, 044616 (2011)
[20] A. Tumino *et al.*, Eur. Phys. J. A direct, 1 (2006) DOI: 10.1140/epja/i2006-08-038-1
[21] R.G. Pizzone *et al.*, Phys. Rev.C **83**, 045801 (2011)
[22] R.G. Pizzone *et al.*, Phys. Rev.C **87**, 025805 (2013)
[23] M.L. Sergi *et al.*, Phys.Rev. C **R82**, 032801 (2010)
[24] M. La Cognata *et al.*, Astrophysical Journal Letters **739**, L54 (2011)
[25] M.L. Sergi *et al.*, Phys.Rev. C **91**, 065803 (2015)
[26] Qun-Gang Wen *et al.*, Phys. Rev.C **78** 035805 (2008)
[27] Qun-Gang Wen *et al.*, J.Phys. G: Nucl. Part. Phys., **38**, 085103 (2011)
[28] A. Tumino *et al.*, Phys. Lett. B **700**, 111 (2011)
[29] M. La Cognata *et al.*, Phys. Rev. Lett. **49**, 015106 (2013)
[30] A. Tumino *et al.*, Astrophysical Journal **785**, 96 (2014)
[31] L. Lamia *et al.*, Astrophysical Journal **768**, 65 (2013)
[32] A. Tumino *et al.*, Astrophysical Journal **785**, 96 (2014)
[33] R.G. Pizzone *et al.*, Astrophysical Journal, **786**,112 (2014)
[34] C. Spitaleri *et al.*, Phys. Rev.C **90**, 035801 (2014)
[35] Li Chengbo *et al.*, Phys. Rev.C **92**, 025805 (2015)
[36] C. Spitaleri *et al.*, Phys. Rev.C **91**, 024612 (2015)
[37] L. LamiaAstrophysical Journal, **850**, 175 (2017)
[38] C. Spitaleri *et al.*, Phys. Rev.C **95**, 035801 (2017)
[39] Li Chengbo *et al.*, Phys. Rev.**95**, 035804 (2017)
[40] G.G. Rapisarda *et al.*, Eur. Phys. J.A **54**, 189 (2018)
[41] L. Lamia *et al.*, Astrophysical Journal, **879**, 23 (2019)
[42] A. Cvetinovic *et al.*, Phys. Rev.C **97**, 065801 (2018)
[43] G.L. Guardo et al., Eur. Phys. J. A **55**, 211 (2019)
[44] R. Spartá et al., Frontiers in Phys. **7**, 560149 (2020)
[45] R.G. Pizzone, C. Spampinato, R. Spartá, et al., Eur. Phys. J. A **56**, 299 (2020)

[46] R. Spartá et al., Eur. Phys. J. A **57**, 170 (2021)
[47] S. Hayakawa *et al.*, Astrophysical Journal Letters **915**, L13 (2021)
[48] R. Spartá et al., Frontiers in Phys. **10**, 896011 (2022)
[49] M. La Cognata *et al.*, Phys. Rev. Lett. **101**, 152501 (2008)
[50] M.L. Sergi *et al.*, Phys.Rev. C **R82**, 032801 (2012)
[51] M. La Cognata *et al.*, Astrophysical Journal **708**, 796 (2010)
[52] M. La Cognata *et al.*, Astrophysical Journal **739**, L54 (2011)
[53] M. La Cognata *et al.*, Phys. Rev. Lett. **49**, 015106 (2013)
[54] M. La Cognata *et al.*, Phys.Rev. C **99**, 034301 (2015)
[55] S. Cherubini *et al.*, Phys. Rev.C **92**, 015805 (2015)
[56] R.G. Pizzone *et al.*, Astrophysical Journal **836**, 57 (2017)
[57] I. Indelicato *et al.*, Astrophysical Journal **845**, 19 2017
[58] G. D'Agata *e*t al., Astrophysical Journal **860**, 61 (2018)
[59] V. Burjan *e*t al., Eur. Phys. J. A **55**, 114 (2019)
[60] S. Palmerini *e*t al., Eur. Phys. J. Plus **136**, 898 (2021)
[61] M. La Cognata *et al.*, Phys. Lett. B **826**, 136917 (2022)
[62] M. La Cognata *et al.*, Astrophysical Journal **941**, 96 (2022)
[63] A. Tumino *e*t al., Nature **557**, 687 (2018).
[64] E. Garcia-Berro *e*t al., Astrophysical Journal, **286**, 765 (1997).
[65] R.L. Cooper *e*t al., Astrophysical Journal, **702**, 660 (2009).
[66] H.W. Becker, K.U. Kettner, C. Rolfs & H.P. Trautvetter, Z. Phys., **303** 305 (1981).
[67] G.R. Caughlan & W.A. Fowler, At. Data Nucl. Data Tables **40**, 283 (1988).
[68] M. Pignatari *e*t al., Astrophysical Journal **762** 31 (2013).
[69] K. Mori *e*t al., Monthly Notices of the Royal Astronomical Society: Letters **482** L70 (2019).
[70] O. Straniero *e*t al., Springer Proceedings in Physics **219**, 7 (2019)
[71] A. Chieffi *e*t al., Astrophysical Journal **916** 79 (2021).
[72] A. Tumino *e*t al., Commun. Phys. **6** 106 (2023).